

See discussions, stats, and author profiles for this publication at: <https://www.researchgate.net/publication/367026090>

Integrated physical approach to assessing urban-scale building photovoltaic potential at high spatiotemporal resolution

Article in Journal of Cleaner Production · February 2023

DOI: 10.1016/j.jclepro.2023.135979

CITATIONS

0

READS

108

4 authors, including:



Zhaoru Liu

Tsinghua University

5 PUBLICATIONS 71 CITATIONS

[SEE PROFILE](#)



Xue Liu

Tsinghua University

12 PUBLICATIONS 140 CITATIONS

[SEE PROFILE](#)



Da Yan

Tsinghua University

237 PUBLICATIONS 7,820 CITATIONS

[SEE PROFILE](#)

Some of the authors of this publication are also working on these related projects:



Project 2019 Researcher Links Workshop on Investigation of the Impact of Occupant Behavior on Building Performance in the UK and China [View project](#)



Project DeST Research & Development [View project](#)

1 Integrated physical approach to assessing urban-scale building photovoltaic
2 potential at high spatiotemporal resolution

3 Zhaoru Liu^a, Xue Liu^a, Haoran Zhang^b, Da Yan^{a,*}

4 ^a*Building Energy Research Center, School of Architecture, Tsinghua University, Beijing 100084, China*

5 ^b*School of Urban Planning and Design, Peking University Shenzhen Graduate School, Shenzhen 518055, China*

6 **Abstract**

7 Assessing the urban-scale building photovoltaic (PV) potential is important for designing urban environments,
8 retrofitting existing structures, or integrating PVs with grids. However, few studies have considered high-temporal-
9 resolution simulations, the facade PV potential, and a comprehensive PV model simultaneously; thus, the overall
10 accuracy of the estimation of PV potential may be limited. Therefore, this study developed an integrated framework to
11 assess the urban-scale PV potential of rooftops and facades at high spatiotemporal resolution. The proposed approach
12 integrates an anisotropic sky diffuse model, a vector-based shading calculation method, and a temperature-related
13 PV performance model. The annual PV potential and spatial/temporal characteristics were analyzed in a case study
14 of over 170,000 buildings in Beijing. The results showed that the estimated rooftop PV power generation was 7.55
15 TWh/y, whereas the facade PV power generation was 18.07 TWh/y, which was 239% of the rooftop PV yield. The
16 integrated model estimated PV yield with higher accuracy than the simplified models by depicting more details. The
17 proposed approach can be applied to the large-scale assessment of future energy systems with increasing penetration
18 of PVs, and the results can support effective policies for the integration of PVs into the built environment in dense
19 cities.

20 **Keywords:** Solar photovoltaic (PV) potential, Spatiotemporal modeling, Solar energy, Roof and facade, Urban
21 building energy modeling

22 **1. Introduction**

23 Cities account for two-thirds of energy consumption and 70% of CO₂ emissions worldwide (IEA, 2021), and ener-
24 gy demand is expected to grow significantly with the rapid urbanization (Molnár et al., 2022). To date, approximately
25 50 countries have achieved or set goals for carbon neutrality in policy documents or laws (Zhang et al., 2022), and
26 many cities are committing to decarbonization in response to national goals (Neij & Heiskanen, 2021). China has also

*Corresponding authors

Email address: yanda@tsinghua.edu.cn (Da Yan)

27 announced the goal of reaching peak CO₂ emissions by 2030 and striving to achieve carbon neutrality by 2060 (Hu
 28 et al., 2022). Mega-cities in China such as Beijing and Shanghai have also proposed targets for peak carbon or carbon
 29 neutrality. However, mega-cities face challenges in the mitigation of carbon emissions (Liu et al., 2022b), especially
 30 in the building sector, which is responsible for even higher carbon emissions than transportation (IPCC, 2015) because
 31 of high building density.

Nomenclature

α	solar altitude angle	IR_{roof}	installation ratio of rooftops
β	slope angle of PV modules	L	projection of sunlight on rooftop
δ	winter solstice solar declination	P_0	rated power of PV panel
γ	solar azimuth angle	S_{facade}	available installation area of facade
ω	winter solstice hour angle	S_{roof}	available installation area of rooftop
ρ	ground surface albedo	SAR	shaded area ratio
σ_{PV}	hourly standard deviation of PV electric power	SVF	sky view factor
θ_{inc}	incident angle	T_a	ambient temperature
θ_z	zenith angle	$T_{a,\text{NOCT}}$	ambient temperature under NOCT test conditions
a, b	geometric angles in Perez model	T_{cell}	PV cell temperature
A_{facade}	total area of facade	T_{ref}	reference temperature
A_{roof}	total area of rooftop	W	width of PV module
E_{PV}	hourly PV electric power	BAPV	building- applied photovoltaic
EUI_c	constraint value of electricity use intensity	BIPV	building-integrated photovoltaic
F_1	circumsolar brightening coefficient	GIS	geographic information system
F_2	horizon brightening coefficient in Perez model	MMH	monthly mean hourly
$G_{b,t}$	direct tilted irradiance component	MPP	maximum power point
$G_{d,t}$	diffuse tilted irradiance component	NOCT	nominal operating cell temperature
$G_{g,t}$	global tilted irradiance component	POA	plane of array
G_{NOCT}	POA irradiance under NOCT test conditions	PV	photovoltaic
$G_{r,t}$	reflected tilted irradiance component	RE	relative error
H	installation height of PV module	STC	standard test conditions
IR_{facade}	installation ratio of facades	TMY	typical meteorological year
		UBEM	urban building energy modeling

32 *1.1. Importance of photovoltaics for decarbonization in building sector*

33 To reduce energy consumption and carbon emissions in the building sector in urban areas, it is important to
34 improve the energy efficiency of buildings and use on-site renewable energy (Panagiotidou et al., 2021). Photovoltaic
35 (PV) deployment in the built environment is a promising way to generate on-site electricity, assuming limited urban
36 space, because there are economically viable areas on roofs and facades for PV deployment (Kuhn et al., 2021).
37 In addition, the electricity is supplied close to the consumption point, reducing transmission and distribution losses
38 (de Sousa Freitas et al., 2020). Building PV systems consist of building-attached PV (BAPV) and building-integrated
39 PV (BIPV) systems. BAPV refers to PV that is simply attached to the building and not used to replace conventional
40 building materials (ISO/TS 18178:2018). This approach is an easy way to retrofit buildings; however, it increases the
41 building load and affects the overall effects of the building (Wang et al., 2016). BIPV refers to photovoltaic materials
42 that are designed to be a component of the building envelope (ISO/TS 18178:2018), which represents an innovative
43 approach that is being rapidly developed (Chen et al., 2019).

44 Since the first attempt to integrate PV systems with the building envelope in the early 1990s, building PV systems
45 have attracted increasing attention (Liu et al., 2021). Research on the integration of PV and buildings aims to improve
46 the module performance (Meng et al., 2022), balance production and consumption (Ceran et al., 2021) and expand
47 application scenarios in different climate zones (Skandalos et al., 2022; Skandalos & Karamanis, 2021).

48 *1.2. Existing research on the assessment of urban-scale building PV potential*

49 From a macro level, the identification of urban-scale building PV potential is also important for designing future
50 urban environments or retrofitting existing structures, and for integrating PV with existing grids (Freitas et al., 2015).
51 However, estimating the PV potential of existing urban building stock is highly challenging (Chatzipoulka et al.,
52 2018). In addition to variable meteorological conditions, the complex urban fabric, building typology and obstructions
53 to incoming sunlight in urban environments also limit the PV potential (Freitas et al., 2015; Horváth et al., 2016).

54 GIS-based estimation can be considered a promising approach to estimating the building PV potential at urban
55 scale, owing to greatly improved computer power and modeling techniques. Gassar & Cha (2021) reviewed the
56 approaches to GIS-based rooftop solar PV potential estimation at urban scale and considered modeling to be the best
57 approach because of its good accuracy, specificity, and potential for automated application, compared with sampling,
58 geostatistics, and machine learning. Table 1 summarizes some existing studies on the assessment of district- or
59 urban-scale building PV potential by physical modeling. Groppi et al. (2018) studied the decrease in non-renewable
60 electricity demand resulting from the deployment of PV systems by combining analyses of electricity generation
61 and consumption. Sun et al. (2022) proposed a framework to assess the PV potential and feasibility on the roofs

62 of urban buildings using a GIS. The electricity self-sufficiency of urban buildings was also analyzed to explore its
63 effect on urban energy security. Xu et al. (2021b) measured the solar energy potential of Hongshan District in Wuhan
64 considering the impact of shade using occlusion factors. A linear regression method was used to obtain the roof solar
65 occlusion factors of urban blocks using the relationships between morphological indicators and occlusion. Cheng
66 et al. (2020) proposed a roof-facade framework to estimate the solar energy potential in 10 cities in China considering
67 shading effects and correcting for weather effects. Panagiotidou et al. (2021) estimated and compared the PV energy
68 potentials of building rooftops, walls, and windows. The relationships between multiple urban form indicators and the
69 PV energy estimates were analyzed. Hong et al. (2017) developed a method for estimating the rooftop PV potential
70 using a raster-based shadow calculation approach, Hillshade. For urban-scale building PV estimation, Walch et al.
71 (2020) provided a methodology for large-scale rooftop PV potential estimation with hourly temporal resolution and a
72 spatial resolution of individual roof surfaces. Florio et al. (2021) assessed the solar energy potential of 473 buildings
73 by combining dynamic energy simulation tools into an open-source computational platform. The simulations included
74 facades, shading by vegetation, and detailed roof shapes.

75 As the summary in Table 1 indicated, current research has not sufficiently considered one or more of the following
76 aspects: high temporal resolution, the potential on facades, and model comprehensiveness. First, an hourly temporal
77 resolution is needed to assess the intraday variation in yield and the impact on the grid (Walch et al., 2020). Hourly
78 profiles of PV yield will support the deployment of energy storage systems. Second, the PV potential of facades
79 is attracting increasing attention (Fath et al., 2015). Facades have larger areas than roofs, especially on multistory
80 buildings. PVs on facades could supplement power generation (Brito et al., 2017). By using PVs on facades with
81 different orientations, the energy production profile can be adjusted to better meet the energy demand (Freitas et al.,
82 2018). Third, a comprehensive model chain is crucial for accurately quantifying the PV potential (Mayer & Gróf,
83 2021).

84 A comprehensive model chain includes the sky diffuse model, PV performance model, and shading calculation
85 (Liao et al., 2022). For sky diffuse model, an anisotropic sky diffuse model exhibits the best performance according
86 to a detailed review (Yang, 2016). For PV efficiency, the cell temperature is a key factor and merits consideration in
87 hourly calculations (Skoplaki & Palyvos, 2009). For shading calculation, pixel-based approaches are commonly used,
88 where building surfaces are divided into pixels, and the sunlight accessibility of each pixel is calculated. However,
89 pixel-based approaches are calculation-intensive. To solve this problem, a sample study can be used to estimate the
90 overall occlusion coefficient (Xu et al., 2021b), or only a representative day of each month can be calculated to reduce
91 the calculation time (Hong et al., 2017; Walch et al., 2020). Besides, a simplified method was proposed to estimate
92 the PV generation of partially shaded PV systems, using shading masks and annual percentage of shading (Zomer &

Table 1: Summary of previous studies on assessment of district- or urban-scale building PV potential by physical modeling.

Reference	Spatial scale	Temporal resolution	Installation position	Model details		
				Sky diffuse model	Shading calculation	PV efficiency
Groppi et al. (2018)	3.2 km ² (land area)	Annual	Rooftop	N/A	N/A	Constant
Sun et al. (2022)	0.43 km ² (rooftop area)	Annual	Rooftop	N/A	Occlusion coefficient	Constant
Xu et al. (2021b)	480 km ² (land area)	Annual	Rooftop	Anisotropic	Occlusion coefficient	Constant
Cheng et al. (2020)	22,594–439,218 (buildings)	Annual	Rooftop and facade	Anisotropic	Pixel-based	Constant
Panagiotidou et al. (2021)	5 km ² (land area)	Annual	Rooftop and facade	Anisotropic	Pixel-based	Constant
Hong et al. (2017)	27,774 (buildings)	Hourly	Rooftop	N/A	Pixel-based	Constant
Walch et al. (2020)	9.6 million (buildings)	Hourly	Rooftop	Anisotropic	Pixel-based	Temperature-related
Florio et al. (2021)	0.56 km ² (land area)	Hourly	Rooftop and facade	N/A	Pixel-based	Temperature-related

93 Rüther, 2017a,b). It may be difficult to calculate the shading of urban building stock year-round.

94 *1.3. Aim and objectives*

95 In light of the above analysis, this study proposes an integrated framework to assess the urban-scale PV potential
96 for building rooftops and facades at a high spatiotemporal resolution using a bottom-up physical modeling approach.
97 It contributes to the literature by achieving the following two objectives:

- 98 • Proposal of a bottom-up physical approach to assessing urban-scale BIPV/BAPV potential at a high spatiotem-
99 poral resolution oriented to urban building energy modeling (UBEM), integrating Perez sky diffuse model,
100 vector-based shading calculation algorithm, and temperature-related PV performance model. Compared with
101 the simplified models, the proposed approach could reflect the magnitude and characteristics of the PV potential
102 with higher accuracy.

- 103 ● Assessment of the PV potential of existing buildings in the mega-city, taking Beijing as an example. The
 104 annual PV potential and the spatiotemporal characteristics of the PV yield are analyzed. The spatial distribution
 105 of annual PV yield is explored and the characteristics of the blocks with high PV potential are investigated.
 106 Appropriate strategies for urban-scale PV deployment are also discussed, including the deployment priority of
 107 rooftops and facades at different azimuths and the selection of buildings and surfaces suitable for deployment.

108 This paper is structured as follows. Section 2 illustrates the workflow of the proposed approach, as well as the input
 109 data and methods used for PV modeling and installation. Section 3 presents the results of PV potential assessment.
 110 Section 4 presents the discussion and Section 5 concludes the main findings.

111 2. Methodology

112 2.1. Input data

113 A 3D city model and meteorological data were input to the framework. The building stock is located in Beijing
 114 (39.8°N, 116.3°E), northern China. The study area covers a ground area of approximately 700 km². The building
 115 footprints were collected from Amap, as shown in Fig. 1(a), with the information of the number of floors above
 116 ground of each building. Historical and scenic buildings accounted for 6,391 of the 180,127 buildings, and were
 117 excluded in determining suitable buildings for PV deployment. The geometry was simplified to 2.5D building blocks
 118 by removing details such as tilted roofs and setbacks with increasing tower height. The height of each building was
 119 generated assuming a floor-to-floor height of 3 m, referring to existing studies on Chinese cities (Deng et al., 2022;
 120 Cheng et al., 2020). The floor area of the building stock has a right-skewed distribution with a median floor area of
 121 1,112 m², as shown in Fig. 1(b). Most buildings in Beijing face south, as shown in Fig. 1(c). The total areas of
 122 rooftops and facades are 114 km² and 249 km² respectively.

123 Beijing has a monsoon-influenced hot-summer humid continental climate and receives approximately 2,700 h
 124 of bright sunshine annually on average, according to historical meteorological data (Liu et al., 2022a). The annual
 125 global horizontal solar irradiance in Beijing is 1,400 kWh/m². Chinese Standard Weather Data were used to assess
 126 the building PV potential (China Meteorological Bureau & Tsinghua University, 2005); these data consist mainly of
 127 normal beam irradiance, horizontal diffuse irradiance, air temperature, and relative humidity in 8,760 h of the year.

128 2.2. Physical PV model

129 PV power is typically calculated using physical, statistical, and hybrid approaches (Mayer & Gróf, 2021). Physical
 130 PV models are useful for PV potential estimation, as they do not require any historical data. However, a model chain
 131 consisting of several calculation steps is crucial for the physical modeling of PV power generation using irradiance

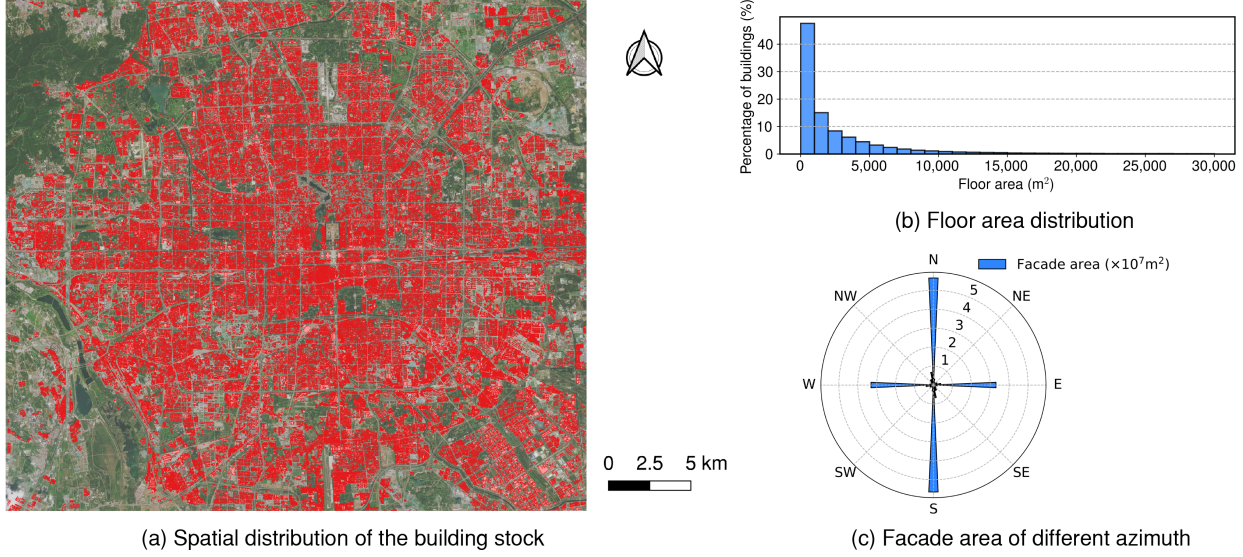


Figure 1: (a) Spatial distribution of the building stock, (b) floor area, and (c) total facade area of building stock in Beijing considered in case study.

132 data. In the proposed model, the plane-of-array (POA) solar irradiance is calculated considering shading effects using
 133 the horizontal irradiance, and then the electricity generation is estimated by the PV performance model.

134 *2.2.1. Irradiance conversion model*

135 The global POA irradiance generally consists of the contributions of three irradiance sources (Duffie et al., 2020),
 136 as follows:

$$G_{g,t} = G_{b,t} + G_{d,t} + G_{r,t} \quad (1)$$

137 where $G_{b,t}$, $G_{d,t}$, and $G_{r,t}$ are the beam, diffuse, and reflected components, respectively. $G_{g,t}$ depends on the incident
 138 angle of solar rays on the PV panel. $G_{b,t}$ is calculated as follows:

$$G_{b,t} = BHI \cdot R_b \quad (2)$$

$$R_b = \begin{cases} \cos \theta_{inc} / \cos \theta_z, & \text{if } \cos \theta_{inc} > 0 \text{ and } \cos \theta_z > 0 \\ 0, & \text{otherwise.} \end{cases} \quad (3)$$

140 where R_b is the contribution of $G_{b,t}$ to the beam horizontal irradiance (BHI), θ_{inc} is the incident angle, and θ_z is the
 141 zenith angle. $G_{d,t}$ is estimated using the anisotropic sky diffuse model by Perez et al. (1988), where $G_{d,t}$ with slope β

¹⁴² has three sources: the sky horizon, sky dome, and circumsolar region.

$$G_{d,t} = DHI \cdot \left[(1 - F_1) \left(\frac{1 + \cos\beta}{2} \right) + F_1 \frac{a}{b} + F_2 \sin\beta \right] \quad (4)$$

¹⁴³ where F_1 and F_2 are the circumsolar brightening coefficient and horizon brightening coefficient obtained by empirical fitting, respectively, and a and b are geometric angles. $G_{r,t}$ is calculated from the surface albedo ρ as follows. The ¹⁴⁴ surface albedo in urban environments is assumed to be 0.3 (Florio et al., 2021), according to the albedo of common ¹⁴⁵ roof and facade materials (MOHURD, 2016).

$$G_{r,t} = GHI \cdot \rho \left(\frac{1 - \cos\beta}{2} \right) \quad (5)$$

¹⁴⁷ Two indicators, the shaded area ratio (*SAR*) and sky view factor (*SVF*), are used to represent the irradiance ¹⁴⁸ reduction by the surroundings. *SAR* is the shaded portion of the building surface calculated for each time step, ¹⁴⁹ which quantifies the accessibility to direct radiation. *SVF* is the visible proportion of the sky. The POA irradiance ¹⁵⁰ considering the surroundings is estimated using Eq. 6.

$$G_{g,t} = (1 - SAR) \cdot G_{b,t} + SVF \cdot G_{d,t} + G_{r,t} \quad (6)$$

¹⁵¹ 2.2.2. Shading calculation

¹⁵² The *SAR* and *SVF* values of each surface are calculated by a geometric projection method, specifically, the ¹⁵³ BShadow algorithm, which is the shadow calculation model in DeST (Yan et al., 2022). The algorithm calculates ¹⁵⁴ *SAR* using the sunlight vector and surface polygons, as follows. First, the hemispherical surface above the target ¹⁵⁵ surface is divided into grids of equal altitude and azimuth. Then the polygonal shadow cast on the target surface ¹⁵⁶ by the surrounding surfaces is calculated, assuming that a light source is present in each grid. The *SAR* values at ¹⁵⁷ each light source position are calculated using this method. Finally, the *SAR* value at each time step throughout a ¹⁵⁸ year is represented by the value at the grid closest to the real sun position. *SVF* is calculated according to the Steyn ¹⁵⁹ method. The sky dome is subdivided into grids, and the visibility of each grid from the viewpoint is determined. ¹⁶⁰ The contribution of each grid to *SVF* is then calculated (Steyn, 1980). To reduce the computational complexity, ¹⁶¹ surrounding buildings whose distance to the target building is less than the height multiplier ($\cot 10^\circ \approx 5.67$) times ¹⁶² the height of the surrounding building were considered as shading elements.

163 2.2.3. PV performance model

164 PV electrical models can be classified as empirical or physical models (Mayer & Gróf, 2021). In empirical
165 models, the maximum power point (MPP), which is regarded as a function of the cell temperature and irradiance,
166 describes the effect of cell temperature and irradiance on the efficiency of a PV module. According to current review
167 of available models, empirical models can describe the relationship between PV performance and operating conditions
168 with sufficient accuracy and high computational efficiency, and the parameters are easily acquired from datasheet
169 information (De la Parra et al., 2017). The PVWatts model is a widely used empirical model that considers the effects
170 of the tilted irradiance and cell temperature on the efficiency at each time step (Dobos, 2014). The formula of the
171 PVWatts model is as follows:

$$P = \frac{G_{g,t}}{1000} P_0 [1 + \gamma (T_{cell} - T_{ref})] \quad (7)$$

172 where P_0 is the rated power of the PV panel, T_{cell} is the cell temperature, and T_{ref} is the reference temperature.

173 Cell temperature significantly affects the efficiency of PV modules, as shown in Eq. 7. The nominal operating cell
174 temperature (NOCT) model is one of the most commonly used models of cell temperature; it assumes that the overall
175 heat transfer can be estimated from the NOCT (Chedid & Saliba, 1996), as shown in Eq. 8.

$$T_{cell} = T_a + \left(\frac{G_{g,t}}{G_{NOCT}} \right) (T_{NOCT} - T_{a,NOCT}) \quad (8)$$

176 where T_a is the ambient temperature, and $G_{NOCT} = 800\text{W/m}^2$ and $T_{a,NOCT} = 20^\circ\text{C}$ are the POA irradiance and
177 ambient temperature under the NOCT test conditions, respectively. Table 2 lists the characteristics of the PV module
178 selected for this study (SolarReviews, 2021). Mono-crystalline silicon PV modules were selected in the potential
179 assessment due to the wide use in China (Zhang et al., 2021).

180 2.3. Installation schemes

181 BIPV/BAPV deployment at urban scale can be affected by many factors, which must be fully considered before
182 the site selection and placement of PV systems. First, to achieve the maximum electricity generation per unit installed
183 capacity, rooftop PV panels should be installed with the optimal tilt angle, and partial shading by PV arrays at the
184 front should be considered (Peng & Lu, 2013). In addition, some uneven areas and areas used for other functions are
185 not suitable for PV deployment; therefore the installation ratio (IR) must be considered. Finally, the total available
186 surface area and solar resources are important for economic reasons, and thus suitable buildings and facades should
187 be selected. These three aspects of installation schemes are described as follows.

Table 2: Characteristics of selected PV module.

Parameter	Value
Rated maximum power (P_0)	530 W
Temperature coefficient of P_0 (γ)	- 0.350%/°C
Nominal operating cell temperature (NOCT)	45±2°C
Reference temperature of Standard Test Conditions (STC) (T_{ref})	25°C
Module efficiency	20.7%
Dimensions ($Length \times Width \times Thickness$)	2256 mm × 1133 mm × 35 mm
Cell orientation	144 (6×24)
Module price	0.3 USD/Wp

188 2.3.1. *Tilt angle and array distance*

189 The tilt angle of PV panels was optimized to maximize the annual solar radiation they receive. The tilt angle
 190 in Beijing was selected as 40°, according to the relevant code (MOHURD, 2012). In addition, the PV panels were
 191 assumed to be installed facing south. Partial shading caused by the front rows will reduce the output power of PV
 192 modules; therefore, it is necessary to reserve a certain space between the front and back rows. The appropriate array
 193 distance was determined to avoid partial shading caused by adjacent rows of PV modules between 9:00 AM and 3:00
 194 PM on the winter solstice in Beijing. The schematic diagram used to calculate the array distance is shown in Fig. 2.
 195 The array distance can be calculated using the projection of sunlight L and solar azimuth angle γ at 9:00 AM on the
 196 winter solstice in Beijing, as follows.

$$D = \cos \gamma \times L \quad (9)$$

197

$$\gamma = \arcsin(\cos \delta \sin \omega / \cos \alpha) \quad (10)$$

198

$$L = H / \tan \alpha \quad (11)$$

199

$$H = W \times \sin \beta \quad (12)$$

200 where δ is the solar declination on the winter solstice, ω is the hour angle at 9:00 AM on the winter solstice, α is the
 201 solar altitude angle, H is the installation height of the PV module, W is the width of the PV module, and β is the tilt

202 angle.

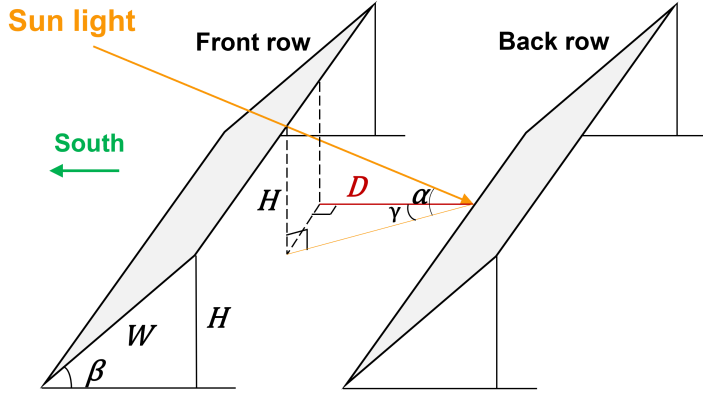


Figure 2: Schematic diagram for calculating the array distance, adapted from Peng & Lu (2013).

203 2.3.2. Installation ratio

204 In urban environments, BIPV/BAPV needs to be coordinated with the building structure, and PV installation must
 205 be avoided on some structures. Facilities and equipment(such as chimneys, ventilation shafts, water tanks, and cooling
 206 towers) occupy parts of the rooftop area (Sun et al., 2022), and the shadows they cast on the rooftops also limit the
 207 available area. Windows, doors, and billboards reduce the available area of facades (Saretta et al., 2020). The PV IR
 208 is commonly used to estimate the available area of rooftops or facades (Panagiotidou et al., 2021).

$$IR_{\text{rooftop}} = \frac{S_{\text{rooftop}}}{A_{\text{rooftop}}} \quad (13)$$

$$IR_{\text{facade}} = \frac{S_{\text{facade}}}{A_{\text{facade}}} \quad (14)$$

209 where S and A are the available and total installation areas of the rooftop or facade, respectively. In this study, the
 210 IRs of rooftops and facades are set to 0.57 and 0.55, respectively, according to previous investigations of buildings in
 211 China (Tian & Xu, 2021; Xu et al., 2021a).

212 2.3.3. Economical deployment

213 To assess the economic potential of BIPV/BAPV, the appropriate deployment strategy is important. Installing PV
 214 panels on all available surfaces may not be cost-efficient. The deployment of BIPV/BAPV requires investment in a
 215 complete system for power generation, conversion, storage, and grid connection, which may be not an economical
 216 option for buildings with a small floor area. Therefore, a lower limit of building floor area was selected, and buildings

217 with floor areas below the lower limit were not considered (Rodríguez et al., 2017). However, the suitability of
 218 building surfaces also affects the annual PV yield, because the insolation of building surfaces depends on shading
 219 effects in urban environments. Therefore, only building surfaces (rooftops or facades) where the solar yield exceeds a
 220 threshold value were considered. The threshold is the minimum solar irradiance required for economical installation
 221 (IEA, 2002). Fig. 3 shows the process of selecting buildings and surfaces for economical PV deployment. First,
 222 buildings with floor areas below the threshold are considered unsuitable for PV deployment. Then the PV yields on
 223 the roofs and facades of each suitable building are calculated and compared with the insolation thresholds for roofs and
 224 facades, respectively. Only surfaces with PV yields per unit area above the threshold are considered in PV potential
 225 assessment. The determination of the floor area and insolation thresholds is described in Section 3.1.

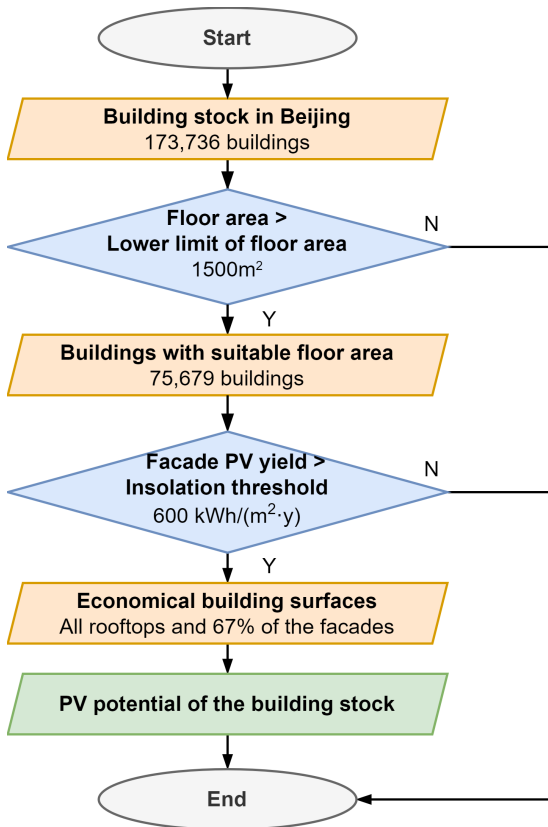


Figure 3: Process of building and surface selection for economical PV deployment.

226 3. Results

227 3.1. Economical installation schemes

228 The strategy described in Section 2.3.3 was used for PV deployment. Fig.4 shows the effect of the minimum
 229 floor area threshold of building stock on the PV yield and number of buildings where PVs are deployed. The number

230 of buildings where PVs are deployed can decrease noticeably without a large decrease in the total PV yield if an
 231 appropriate lower limit of the building floor area is selected. The floor area threshold was set to 1,500 m², at which
 232 over 85% of the total yield can be maintained with PV deployment on less than 45% of the buildings. According to
 233 the floor area threshold, 75,679 buildings were chosen for further PV deployment.

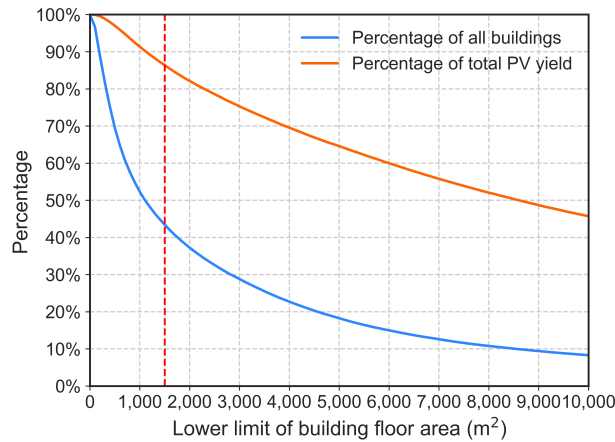


Figure 4: Effect of minimum roof area on PV yield and number of buildings selected.

234 The annual PV yield per unit area of building roofs or facades was used to represent the insolation threshold. Fig.
 235 5 shows the total area of roofs/facades and total PV yield as a function of insolation threshold. As shown in Fig.
 236 5(a), both the total area and PV yield decrease sharply at an insolation threshold of 1,500 kWh/(m²·y), indicating that
 237 the dispersion of annual PV yield on rooftops is quite small. In addition, it is hard to select an insolation threshold
 238 for roofs that minimizes the installed capacity without reducing the total PV yield, because the two curves almost
 239 overlap. The insolation threshold for facades was determined according to Fig. 5(b). The area of facades with annual
 240 PV yields exceeding 600 kWh/(m²·y) accounted for 67% of the total facade area, and the PV yield accounted for 82%
 241 of the total PV yield of the facades.

242 3.2. Electricity generation at urban scale

243 3.2.1. Installed capacity and annual PV yield

244 The PV potential of rooftops and facades at urban scale were analyzed considering the installed capacity and
 245 the corresponding PV power generation. As shown in Table 3, south facades have the largest PV power generation,
 246 followed by rooftops, west facades, east facades, and north facades. South facades have the largest installed PV
 247 capacity because of the large available facade area. The power generation and installed capacity of rooftops are
 248 smaller, because the tilt angle of PV panels is considered, and distance between panels is reserved to eliminate shading
 249 effects. The ratio of annual PV power generation to installed capacity represents the full load hours of rooftops and

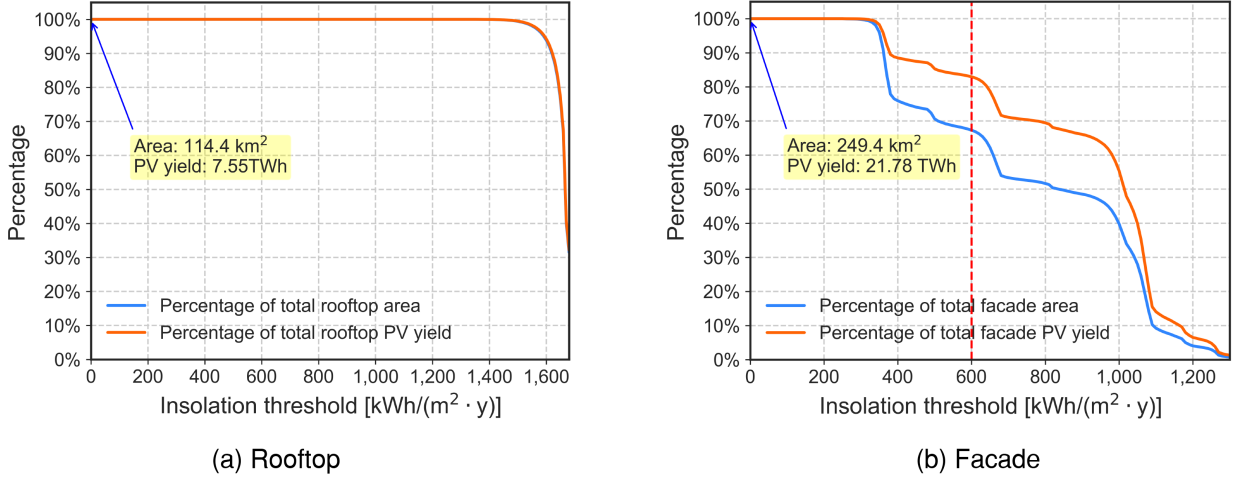


Figure 5: Effect of insolation threshold on PV yield of (a) rooftops and (b) facades.

250 facades, which are the total annual PV yield per unit of installed capacity. PVs on rooftops have the highest full
 251 load hours, followed by south, west, east, and north facades, indicating the solar accessibility of rooftops and facades
 252 with different azimuths. The installed capacity and total annual PV power generation are listed in Table 3. Facades
 253 in urban built environments also have excellent PV potential, in addition to rooftops. The PV power generation of
 254 facades was 18.07 TWh/y, which was 239% of the rooftop PV yield. The abundant solar energy resources on the
 255 facades of building stock in Beijing are expected to play an important role in urban decarbonization.

Table 3: Installed capacity and annual PV power generation of rooftops and facades.

Type	Azimuth γ^*	Installed capacity (GW)	Annual PV power generation (TWh/y)	Full load hours (h)
Rooftop	\	4.72	7.55	1599
South facade	$315^\circ < \gamma \leq 360^\circ$ or $0^\circ < \gamma \leq 45^\circ$	9.02	9.58	1062
West facade	$45^\circ < \gamma \leq 135^\circ$	5.27	5.16	979
East facade	$225^\circ < \gamma \leq 315^\circ$	4.70	3.23	687
North facade	$135^\circ < \gamma \leq 225^\circ$	0.15	0.10	667

* Due south is 0° , and the clockwise direction is positive.

256 3.2.2. Temporal characteristics of PV electricity generation

257 Fig. 6(a) shows the temporal variation in PV potential on rooftops and facades at urban scale. The monthly mean
 258 hourly (MMH) profiles of PV electricity generation are shown to indicate the temporal characteristics while avoiding
 259 the effects of volatility. Each MMH time step represents an average value across all days of the month at a given hour.
 260 The standard deviation σ_{PV} is also shown on both sides of the profiles of E_{PV} to indicate the diurnal variability. The
 261 electricity yield of rooftop PVs is similar for all months. However, facade PVs generate more electricity in winter

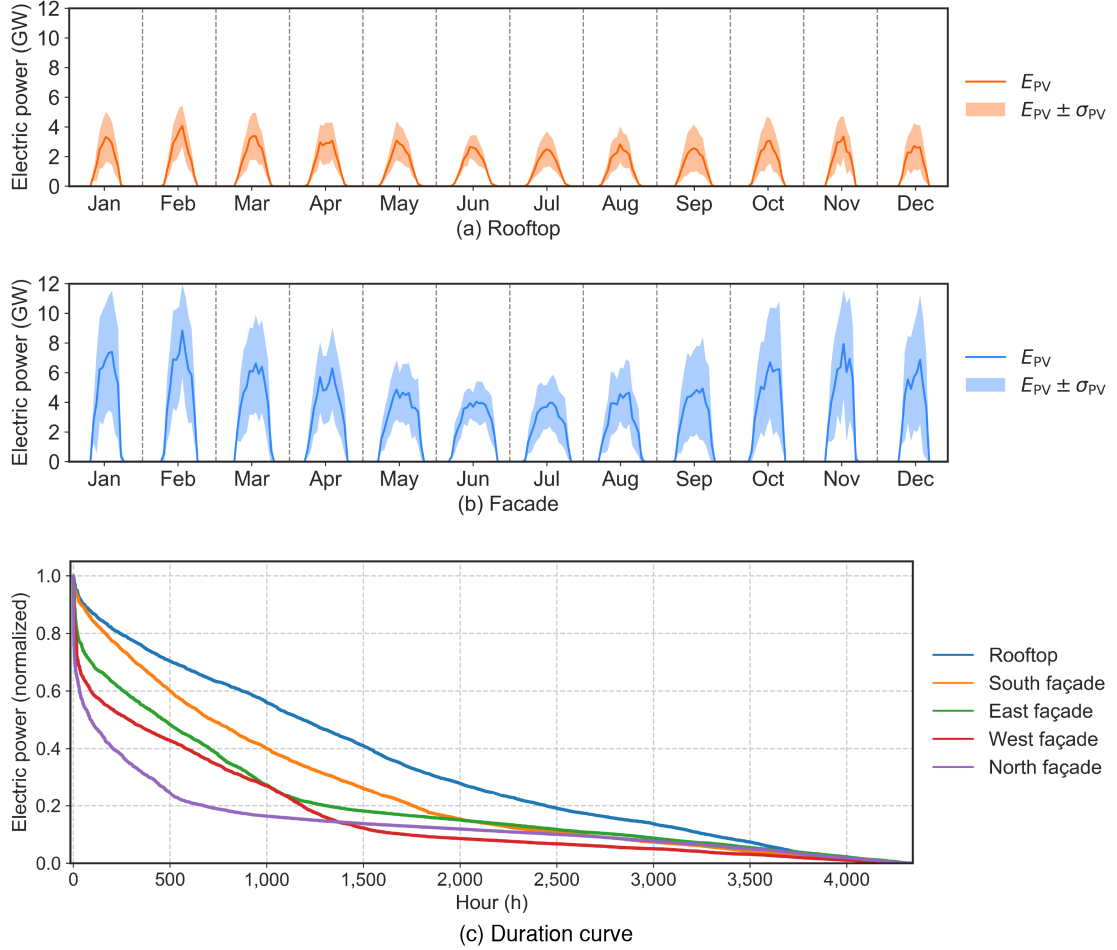


Figure 6: Temporal characteristics of PV electricity generation: MMH profiles of PV yield (E_{PV}) and standard deviation (σ_{PV}) on (a) rooftops and (b) facades, and (c) duration curves of rooftops and facades.

than in summer, because the solar altitude is higher, and the solar irradiance on south facades is smaller in summer than in winter. The MMH profiles of rooftops and facades in the morning and afternoon are symmetrical. Facade PVs have even greater potential than rooftop PVs because of the larger available area, as revealed by the comparison of rooftops and facades. As shown by σ_{PV} in Fig. 6(a), PV electricity generation varies because of the variability in weather conditions, which is an important issue in urban-scale PV deployment.

To show the annual distribution of electric power, the duration curves of rooftops and facades are shown in Fig. 6(c). The electric power curves are normalized by the maximum for better comparison with the temporal distribution (Zhan et al., 2020). The duration curves of facades show a sharp decrease when the electric power is high, indicating that hours with high PV power account for a small proportion of the entire year. Specifically, there are less than 1,000 h in the year when the electric power of facade PVs exceeds 40% of the maximum power, whereas there are approximately 1,500 h in which the electric power of rooftop PVs exceeds 40% of the maximum value. The duration

273 curve of rooftop PVs lies above that of facades during most hours of the year, indicating that electric power production
274 by rooftop PVs exhibits less variation than that of facade PVs.

275 *3.2.3. Spatial distribution of PV electricity generation*

276 The studied area was divided into grid units with dimensions of 500 m × 500 m. The building PV electricity
277 generation on rooftops or facades in each grid was calculated by aggregation to show the PV yield at the block scale.
278 Fig. 7(a) shows the spatial distribution of the annual PV yield on rooftops per grid. Lighter and darker areas represent
279 low and high PV yields, respectively. Grids with higher rooftop PV yields are located both downtown and in suburbs,
280 and there is no significant difference between downtown and the surrounding areas. To explain this result, Fig. 7(b)
281 shows two typical blocks with high rooftop PV yields and the PV yields of each building. One type of block with high
282 rooftop PV yields has high building density, which is common downtown with many low-rise or middle-rise offices,
283 hotels, and apartments. Although the roof area of each building is limited, the number of buildings is large. The other
284 type has buildings with large roofs, such as industrial plants, transportation hubs, and shopping malls. Therefore,
285 industrial campuses in the suburbs may have high rooftop PV yields.

286 Similarly, Fig. 8(a) shows the spatial distribution of annual PV yield on facades per grid. Downtown blocks have
287 higher facade PV yields than those in suburbs since the building height and density are higher in downtown. Fig. 8(b)
288 shows the block fabric and facade PV yields of each building in two typical blocks with high facade PV yields. One
289 type of block with high facade PV yields, which appears mainly in the central business district, has high-rise buildings
290 with abundant available facade areas. The other type has high building density. Smaller distances are needed between
291 low-rise buildings, and thus more buildings in the block can be used for PVs.

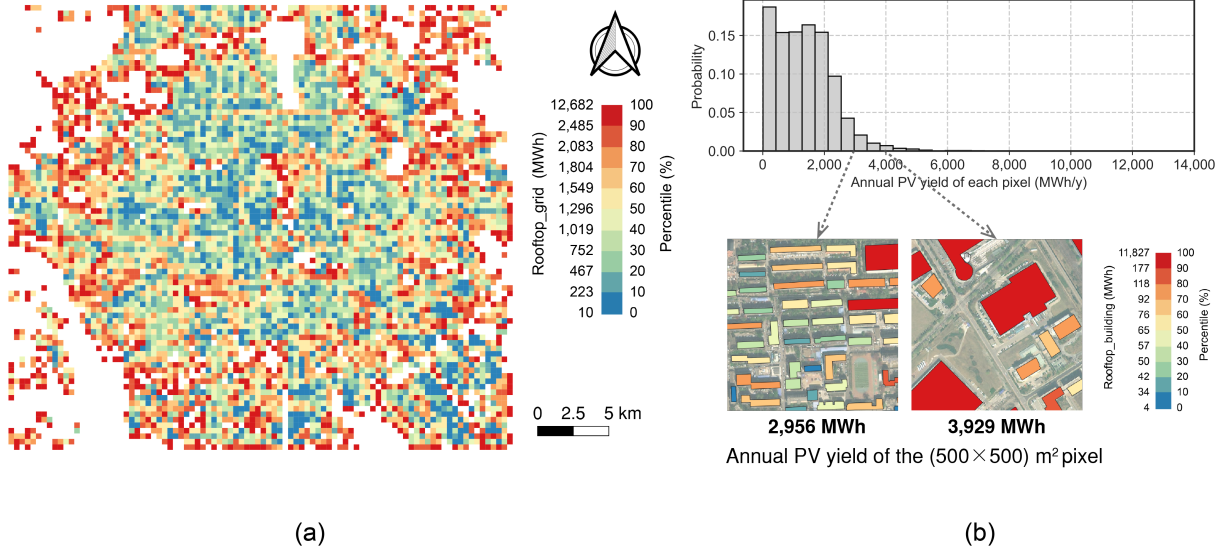


Figure 7: Spatial characteristics of rooftop PV yield: (a) spatial distribution of annual rooftop PV yield, aggregated to pixels of $500 \times 500 \text{ m}^2$ for visualization and (b) histogram of annual rooftop PV yield of each pixel and annual rooftop PV yield of suitable roofs on two typical high-yield blocks.

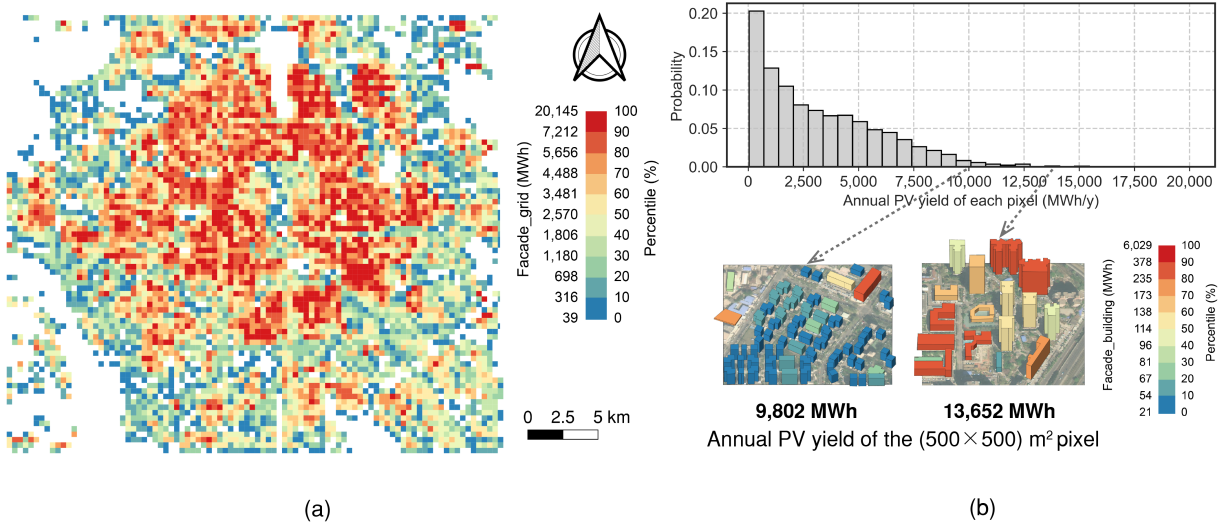


Figure 8: Spatial characteristics of facade PV yield: (a) spatial distribution of annual facade PV yield, aggregated to pixels of $500 \times 500 \text{ m}^2$ for visualization and (b) histogram of annual facade PV yield of each pixel and annual facade PV yield of suitable facades in two typical high-yield blocks.

292 4. Discussion

293 4.1. Impact of sky diffuse model, shading and PV efficiency on urban-scale PV potential

294 In this study, a comprehensive model was proposed which integrated high-accuracy sky diffuse model, vector-based shading calculation algorithm and temperature-related PV performance model. To further demonstrate the

improved accuracy of the proposed model, the proposed model was compared with three simplified models: (a) Without shading: the shading effect was neglected (i.e. $SAR = 0$ and $SVF = 1$); (b) Constant efficiency: the effect of cell temperature on PV efficiency was neglected and a constant PV efficiency (20.7%) was set; (c) Isotropic diffuse: an isotropic sky diffuse model (Liu & Jordan, 1960) was utilized to calculate $G_{d,t}$.

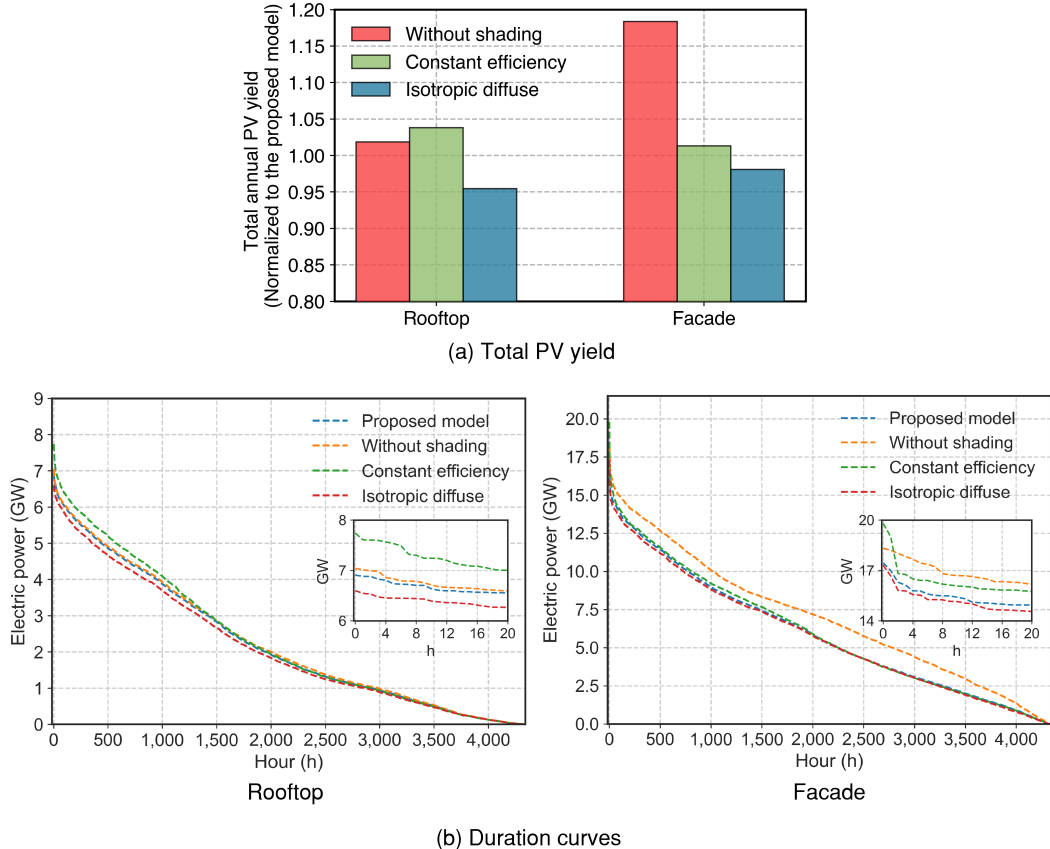


Figure 9: Comparison of (a) total annual PV yield, and (b) duration curves between the proposed model and simplified models. The first 20 hours of the duration curves are shown separately.

Total annual PV yields of the three simplified models were normalized to that of the proposed comprehensive model, as shown in Fig. 9(a). The duration curves of the proposed model and three simplified models were shown in Fig. 9(b). There are two key findings in the comparison between the simplified models and the proposed model. First, simplification of any one component of the model may lead to discrepancy in the annual PV yield, duration curves, and peak power. The estimated annual PV yield may vary between 95% and 118% of the proposed model results. The duration curves of simplified models all showed different characteristics from the proposed model. Peak power may be significantly overestimated when the PV efficiency is considered constant. Second, the key influences of rooftop and facade are different for both annual PV potential and duration curves. For rooftop, the estimated annual rooftop PV yield changed most when anisotropy in sky diffuse model was neglected, followed by neglecting efficiency

309 variation and shading effect. However, for facade, the annual PV yield may be overestimated by 18% when neglecting
 310 shading effects, much higher than the effects of the other two factors. For facade, the duration curve without shading
 311 changes significantly compared to the proposed model, while for rooftop, the sky diffuse model and PV performance
 312 model have a greater effect on the duration curve than shading. Therefore, the proposed model integrated detailed
 313 models for sky diffuse, shading calculation, and PV performance, and could assess PV potential with higher accuracy.

314 *4.2. Comparison of electricity generation and consumption according to building type*

315 As shown by the above results, the roofs and facades of urban building stock have excellent potential for PV power
 316 generation. However, for the use of distributed PVs, it is also important to analyze the potential for self consumption.
 317 A sample of 200 buildings of each type was randomly selected, and their annual PV yields per unit floor area were
 318 compared with the constraint value of electricity use intensity (EUI_c) excluding heating from the Standard for Energy
 319 Consumption of Buildings (GB/T 51161-2016), as shown in Fig. 10 (Yan et al., 2017). For residences and offices, the
 320 average PV yield of rooftops is higher than that of facades. However, the average PV yield of rooftops exceeds that
 321 of facades for shopping malls, which have larger roof areas than residences and offices.

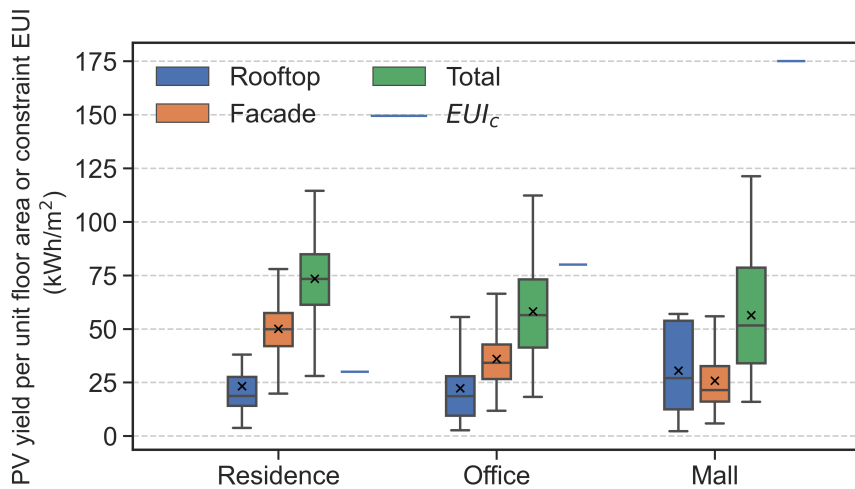


Figure 10: Comparison of electricity generation and consumption by building type. The boxplots represent PV yield, and the short lines represent the constraint values of electricity consumption, excluding heating.

322 A comparison of PV yields with electricity consumption reveals that 16% of the sampled residences could generate
 323 more PV electricity than they consume, using rooftops. The percentage increased significantly when both rooftops
 324 and facades were considered. For offices, rooftop or facade PVs alone could barely satisfy the electricity demand.
 325 When PVs on both rooftops and facades were considered, the PV yields of 19% of the offices exceed the EUI_c . The
 326 EUI_c of shopping malls is much higher than the annual total PV yields. None of the sampled shopping malls could
 327 satisfy the EUI_c value of shopping malls.

328 *4.3. Comparison with the results of similar studies*

329 The estimates of the PV potential of this study were compared with similar studies in Beijing to validate the
 330 proposed approach, as shown in Table 4. The electricity generation and installed capacity of tilted rooftop PV in this
 331 study are similar to those in the existing studies, and the installed capacity per unit area is close to the recommendation
 332 for rooftop PV project of the Ministry of Natural Resources (MNR) of China ($21\text{m}^2/\text{kW}$). Fewer studies assessed the
 333 PV potential on facades compared with rooftops, and the results in this study are close to those by Cheng et al. (2020).

Table 4: Comparisons with the results of similar studies in Beijing.

Reference	Descriptions	Installation	Electricity [kWh/(m ² .y)]	Installed capacity (W/m ²)
Zhang et al. (2020)	The installed capacity was estimated using the average land use, and the power generation was estimated using utilization hours and installed capacity.	Rooftop: tilted	57.7	47.6
Zhang et al. (2021)	The optimal tilt angle and installation spacing were considered, and the PV efficiency was assumed constant.	Rooftop: tilted	75.0	42.0
Cheng et al. (2020)	The power generation was estimated assuming flat roofs and constant PV efficiency, considering shading.	Rooftop: horizontal	198.4	N/A
This study		Rooftop: tilted	66.0	41.2
Cheng et al. (2020)	The power generation was estimated using constant PV efficiency, considering shading.	Facade: vertical	119.2	N/A
This study		Facade: vertical	131.7	76.8

334

335 *4.4. Limitations and potential further investigations*

336 There are some limitations of this study. First, the PV deployment should be in line with local circumstances con-
 337 sidering architectural aesthetics or constructive issues (Polo López et al., 2021), and some compromises are inevitable
 338 considering the shape of the buildings and the PV systems. Specific criteria for selecting appropriate buildings and
 339 technologies could be applied in the proposed approach to estimate the potential of PV installation and power gener-
 340 ation more accurately (Lucchi, 2022).

341 Second, the floor-to-floor height and the rooftop and facade typology are assumed homogeneous in the building
 342 stock, and their variation may affect both the shading effect and facade PV installation, leading to discrepancies
 343 between estimates and actual situations. More detailed building characteristics could improve the accuracy of the
 344 assessment. Besides, the impact of surrounding influences on PV potential also needs further investigation, such as
 345 trees (Sun et al., 2021).

346 Third, the insolation threshold of PV deployment may change with the necessity to mitigate climate change and
 347 technological advances, and the installation conditions of building surfaces may be improved by some appropriate

348 retrofits. The variation of insolation threshold and IR may affect the annual PV yield, as shown in Fig. 11. Therefore,
 349 more scenarios should be further analyzed, integrating climate impacts, technology, and economics.

350 Fourth, a hybrid model combining physical modeling and machine learning is expected to improve accuracy.
 351 Nowadays, novel networks have been proposed for accurate geo-object segmentation from satellite imagery, which
 352 will contribute to available area estimation and shading calculation (Li et al., 2021).

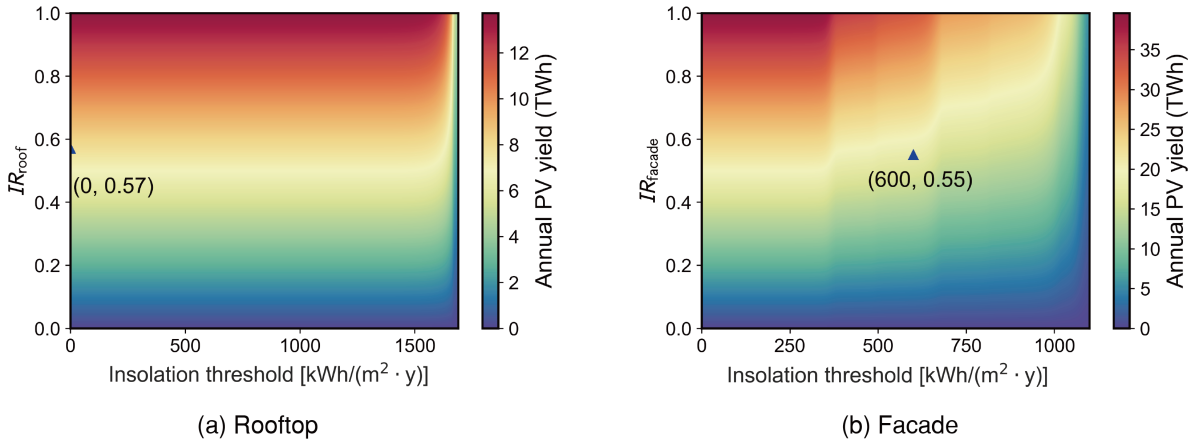


Figure 11: Annual PV yield of (a) rooftops and (b) facades under the variation of insolation threshold and IR. The calculation conditions in this study are marked.

353 5. Conclusion

354 This study developed an integrated physical approach to assessing urban-scale building PV potential. The main
 355 findings in this study are as follows:

- 356 • The bottom-up, physical approach could reflect more details in sky diffuse, shading calculation, and PV perfor-
 357 mance, which could assess urban-scale PV potential with higher accuracy.
- 358 • The urban-scale PV potential of rooftops and facades was estimated in Beijing. The facades were found to have
 359 considerable solar energy resources that merit utilization. The PV potential of south facades was even greater
 360 than that of rooftops. The results showed that the estimated rooftop PV power generation was 7.55 TWh/y,
 361 whereas the facade PV power generation was 18.07 TWh/y, which was 239% of the rooftop PV yield.
- 362 • The spatial distributions and temporal characteristics of the PV yields of rooftops and facades were also ana-
 363 lyzed. PV potential on facades was greater in downtown Beijing than in suburbs, while the PV potential on
 364 rooftops were similar. The blocks with high rooftop PV potential usually have high building density or build-

365 ings with large roofs, and the blocks with high facade PV potential often have high building density or high-rise
366 buildings.

367 The work presented in this study could support decarbonization policies in Beijing, as it enables the urban-scale
368 modeling of future electricity grids with high penetration of building PVs using hourly data for individual buildings.
369 The framework of PV potential assessment could be extended to other regions with sufficient input data, where it can
370 contribute to the transition to low-carbon energy systems.

371 **Acknowledgements**

372 This study was supported by the National Natural Science Foundation of China (Grant Number: 52225801) and
373 Beijing Municipal Natural Science Foundation of China (Grant number 8222019).

374 **References**

- 375 Brito, M., Freitas, S., Guimarães, S., Catita, C., & Redweik, P. (2017). The importance of facades for the solar pv potential of a mediterranean city
376 using lidar data. *Renewable Energy*, 111, 85–94.
- 377 Ceran, B., Jurasz, J., Mielcarek, A., & Campana, P. E. (2021). Pv systems integrated with commercial buildings for local and national peak load
378 shaving in poland. *Journal of Cleaner Production*, 322, 129076.
- 379 Chatzipoulka, C., Compagnon, R., Kaempf, J., & Nikolopoulou, M. (2018). Sky view factor as predictor of solar availability on building façades.
380 *Solar Energy*, 170, 1026–1038.
- 381 Chedid, R., & Saliba, Y. (1996). Optimization and control of autonomous renewable energy systems. *International Journal of Energy Research*,
382 20, 609–624.
- 383 Chen, X., Huang, J., Yang, H., & Peng, J. (2019). Approaching low-energy high-rise building by integrating passive architectural design with
384 photovoltaic application. *Journal of Cleaner Production*, 220, 313–330.
- 385 Cheng, L., Zhang, F., Li, S., Mao, J., Xu, H., Ju, W., Liu, X., Wu, J., Min, K., Zhang, X. et al. (2020). Solar energy potential of urban buildings in
386 10 cities of china. *Energy*, 196, 117038.
- 387 China Meteorological Bureau, & Tsinghua University (2005). *China Standard Weather Data for Analyzing Building Thermal Conditions*. China
388 Architecture and Building Press.
- 389 Deng, Z., Chen, Y., Yang, J., & Chen, Z. (2022). Archetype identification and urban building energy modeling for city-scale buildings based on gis
390 datasets. *Building Simulation*, 15, 1547 – 1559.
- 391 Dobos, A. P. (2014). *PVWatts version 5 manual*. Technical Report National Renewable Energy Lab.(NREL), Golden, CO (United States).
- 392 Duffie, J. A., Beckman, W. A., & Blair, N. (2020). *Solar engineering of thermal processes, photovoltaics and wind*. John Wiley & Sons.
- 393 Fath, K., Stengel, J., Sprenger, W., Wilson, H. R., Schultmann, F., & Kuhn, T. E. (2015). A method for predicting the economic potential of
394 (building-integrated) photovoltaics in urban areas based on hourly radiance simulations. *Solar energy*, 116, 357–370.
- 395 Florio, P., Peronato, G., Perera, A., Di Blasi, A., Poon, K. H., & Kämpf, J. H. (2021). Designing and assessing solar energy neighborhoods from
396 visual impact. *Sustainable Cities and Society*, 71, 102959.
- 397 Freitas, S., Catita, C., Redweik, P., & Brito, M. C. (2015). Modelling solar potential in the urban environment: State-of-the-art review. *Renewable
398 and Sustainable Energy Reviews*, 41, 915–931.

- 399 Freitas, S., Reinhart, C., & Brito, M. (2018). Minimizing storage needs for large scale photovoltaics in the urban environment. *Solar Energy*, *159*,
400 375–389.
- 401 Gassar, A. A. A., & Cha, S. H. (2021). Review of geographic information systems-based rooftop solar photovoltaic potential estimation approaches
402 at urban scales. *Applied Energy*, *291*, 116817.
- 403 Groppi, D., de Santoli, L., Cumo, F., & Astiaso Garcia, D. (2018). A gis-based model to assess buildings energy consumption and usable solar
404 energy potential in urban areas. *Sustainable Cities and Society*, *40*, 546–558.
- 405 Hong, T., Lee, M., Koo, C., Jeong, K., & Kim, J. (2017). Development of a method for estimating the rooftop solar photovoltaic (pv) potential by
406 analyzing the available rooftop area using hillshade analysis. *Applied Energy*, *194*, 320–332.
- 407 Horváth, M., Kassai-Szoó, D., & Csoknyai, T. (2016). Solar energy potential of roofs on urban level based on building typology. *Energy and
408 Buildings*, *111*, 278–289.
- 409 Hu, S., Zhang, Y., Yang, Z., Yan, D., & Jiang, Y. (2022). Challenges and opportunities for carbon neutrality in china's building sector—modelling
410 and data. *Building Simulation*, *15*, 1899–1821.
- 411 IEA (2021). *Empowering Cities for a Net Zero Future: Unlocking Resilient, Smart, Sustainable Urban Energy Systems*. OECD Publishing.
- 412 IEA, P. (2002). Potential for building integrated photovoltaics. *Report IEAPVPS T7-4 Summary*; [Online] Available, ; www.iea-pvps.org/; [accessed
413 02.11.14]. .
- 414 IPCC (2015). Buildings. In *Climate Change 2014: Mitigation of Climate Change: Working Group III Contribution to the IPCC Fifth Assessment
415 Report* (p. 671–738). Cambridge University Press.
- 416 ISO/TS 18178:2018 (2018). *Glass in building – Laminated solar photovoltaic glass for use in buildings*. Standard International Organization for
417 Standardization Geneva, CH.
- 418 Kuhn, T. E., Erban, C., Heinrich, M., Eisenlohr, J., Ensslen, F., & Neuhaus, D. H. (2021). Review of technological design options for building
419 integrated photovoltaics (bipv). *Energy and Buildings*, *231*, 110381.
- 420 Li, P., Zhang, H., Guo, Z., Lyu, S., Chen, J., Li, W., Song, X., Shibusaki, R., & Yan, J. (2021). Understanding rooftop pv panel semantic
421 segmentation of satellite and aerial images for better using machine learning. *Advances in applied energy*, *4*, 100057.
- 422 Liao, W., Xu, S., & Heo, Y. (2022). Evaluation of model fidelity for solar analysis in the context of distributed pv integration at urban scale.
423 *Building Simulation*, .
- 424 Liu, B. Y., & Jordan, R. C. (1960). The interrelationship and characteristic distribution of direct, diffuse and total solar radiation. *Solar Energy*, *4*,
425 1–19.
- 426 Liu, S., Xie, Y., Zhu, Y., Lin, B., Cao, B., Wong, N. H., Niu, J., Fang, Z., Lai, D., Liu, W. et al. (2022a). Comparative analysis on indoor and
427 outdoor thermal comfort in transitional seasons and summer based on multiple databases: Lessons learnt from the outdoors. *Science of The
428 Total Environment*, *848*, 157694.
- 429 Liu, Z., Zhang, Y., Yuan, X., Liu, Y., Xu, J., Zhang, S., & jie He, B. (2021). A comprehensive study of feasibility and applicability of building
430 integrated photovoltaic (bipv) systems in regions with high solar irradiance. *Journal of Cleaner Production*, *307*, 127240.
- 431 Liu, Z., Zhou, X., Tian, W., Liu, X., & Yan, D. (2022b). Impacts of uncertainty in building envelope thermal transmittance on heating/cooling
432 demand in the urban context. *Energy and Buildings*, *273*, 112363.
- 433 Lucchi, E. (2022). Integration between photovoltaic systems and cultural heritage: A socio-technical comparison of international policies, design
434 criteria, applications, and innovation developments. *Energy Policy*, *171*, 113303.
- 435 Mayer, M. J., & Gróf, G. (2021). Extensive comparison of physical models for photovoltaic power forecasting. *Applied Energy*, *283*, 116239.
- 436 Meng, Y., Tan, Y., Li, X., Cai, Y., Peng, J., & Long, Y. (2022). Building-integrated photovoltaic smart window with energy generation and
437 conservation. *Applied Energy*, *324*, 119676.

- 438 MOHURD (2012). Code for design of photovoltaic power station (GB 50797-2012).
- 439 MOHURD (2016). Code for thermal design of civil building (GB 50176-2016).
- 440 Molnár, G., Ürge Vorsatz, D., & Chatterjee, S. (2022). Estimating the global technical potential of building-integrated solar energy production
441 using a high-resolution geospatial model. *Journal of Cleaner Production*, 375, 134133.
- 442 Neij, L., & Heiskanen, E. (2021). Municipal climate mitigation policy and policy learning - a review. *Journal of Cleaner Production*, 317, 128348.
- 443 Panagiotidou, M., Brito, M. C., Hamza, K., Jasieniak, J. J., & Zhou, J. (2021). Prospects of photovoltaic rooftops, walls and windows at a city to
444 building scale. *Solar Energy*, 230, 675–687.
- 445 De la Parra, I., Muñoz, M., Lorenzo, E., García, M., Marcos, J., & Martínez-Moreno, F. (2017). PV performance modelling: A review in the light
446 of quality assurance for large PV plants. *Renewable and Sustainable Energy Reviews*, 78, 780–797.
- 447 Peng, J., & Lu, L. (2013). Investigation on the development potential of rooftop pv system in hong kong and its environmental benefits. *Renewable
448 and sustainable energy reviews*, 27, 149–162.
- 449 Perez, R., Stewart, R., Seals, R., & Guertin, T. (1988). *The development and verification of the Perez diffuse radiation model*. Technical Report
450 Sandia National Lab.(SNL-NM), Albuquerque, NM (United States); State Univ
- 451 Polo López, C. S., Lucchi, E., Leonardi, E., Durante, A., Schmidt, A., & Curtis, R. (2021). Risk-benefit assessment scheme for renewable solar
452 solutions in traditional and historic buildings. *Sustainability*, 13.
- 453 Rodríguez, L. R., Duminil, E., Ramos, J. S., & Eicker, U. (2017). Assessment of the photovoltaic potential at urban level based on 3d city models:
454 A case study and new methodological approach. *Solar Energy*, 146, 264–275.
- 455 Saretta, E., Bonomo, P., & Frontini, F. (2020). A calculation method for the bipv potential of swiss façades at lod2. 5 in urban areas: A case from
456 ticino region. *Solar Energy*, 195, 150–165.
- 457 Skandalos, N., & Karamanis, D. (2021). An optimization approach to photovoltaic building integration towards low energy buildings in different
458 climate zones. *Applied Energy*, 295, 117017.
- 459 Skandalos, N., Wang, M., Kapsalis, V., D'Agostino, D., Parker, D., Bhuvad, S. S., Udayraj, Peng, J., & Karamanis, D. (2022). Building pv
460 integration according to regional climate conditions: Bipv regional adaptability extending köppen-geiger climate classification against urban
461 and climate-related temperature increases. *Renewable and Sustainable Energy Reviews*, 169, 112950.
- 462 Skoplaki, E., & Palyvos, J. A. (2009). Operating temperature of photovoltaic modules: A survey of pertinent correlations. *Renewable energy*, 34,
463 23–29.
- 464 SolarReviews (2021). LR5-72HPH-530M solar panel from LONGi Solar: specs, prices and reviews. Retrieved from <https://www.solarreviews.com/manufacturers/longi-solar/solar-panels/f46631b791himo51r572hph530m>. Assessed October 10, 2022.
- 466 de Sousa Freitas, J., Cronemberger, J., Soares, R. M., & Amorim, C. N. D. (2020). Modeling and assessing bipv envelopes using parametric
467 rhinoceros plugins grasshopper and ladybug. *Renewable Energy*, 160, 1468–1479.
- 468 Steyn, D. (1980). The calculation of view factors from fisheye-lens photographs: Research note. *Atmosphere-Ocean*, 18, 254–258.
- 469 Sun, H., Heng, C. K., Tay, S. E. R., Chen, T., & Reindl, T. (2021). Comprehensive feasibility assessment of building integrated photovoltaics (bipv)
470 on building surfaces in high-density urban environments. *Solar Energy*, 225, 734–746.
- 471 Sun, L., Chang, Y., Wu, Y., Sun, Y., & Su, D. (2022). Potential estimation of rooftop photovoltaic with the spatialization of energy self-sufficiency
472 in urban areas. *Energy Reports*, 8, 3982–3994.
- 473 Tian, J., & Xu, S. (2021). A morphology-based evaluation on block-scale solar potential for residential area in central china. *Solar Energy*, 221,
474 332–347.
- 475 Walch, A., Castello, R., Mohajeri, N., & Scartezzini, J.-L. (2020). Big data mining for the estimation of hourly rooftop photovoltaic potential and
476 its uncertainty. *Applied Energy*, 262, 114404.

- 477 Wang, W., Liu, Y., Wu, X., Xu, Y., Yu, W., Zhao, C., & Zhong, Y. (2016). Environmental assessments and economic performance of bapv and bipv
478 systems in shanghai. *Energy and Buildings*, 130, 98–106.
- 479 Xu, S., Jiang, H., Xiong, F., Zhang, C., Xie, M., & Li, Z. (2021a). Evaluation for block-scale solar energy potential of industrial block and
480 optimization of application strategies: A case study of wuhan, china. *Sustainable Cities and Society*, 72, 103000.
- 481 Xu, S., Li, Z., Zhang, C., Huang, Z., Tian, J., Luo, Y., & Du, H. (2021b). A method of calculating urban-scale solar potential by evaluating and
482 quantifying the relationship between urban block typology and occlusion coefficient: A case study of wuhan in central china. *Sustainable Cities
483 and Society*, 64, 102451.
- 484 Yan, D., Hong, T., Li, C., Zhang, Q., An, J., & Hu, S. (2017). A thorough assessment of china's standard for energy consumption of buildings.
485 *Energy and Buildings*, 143, 114–128.
- 486 Yan, D., Zhou, X., An, J., Kang, X., Bu, F., Chen, Y., Pan, Y., Gao, Y., Zhang, Q., Zhou, H. et al. (2022). DeST 3.0: A new-generation building
487 performance simulation platform. *Building Simulation*, .
- 488 Yang, D. (2016). Solar radiation on inclined surfaces: Corrections and benchmarks. *Solar Energy*, 136, 288–302.
- 489 Zhan, S., Liu, Z., Chong, A., & Yan, D. (2020). Building categorization revisited: A clustering-based approach to using smart meter data for
490 building energy benchmarking. *Applied energy*, 269, 114920.
- 491 Zhang, W., Huang, F., Mao, K., Lin, C., & Pan, Z. (2021). Evaluation of photovoltaic energy saving potential and investment value of urban
492 buildings in china based on gis technology. *Buildings*, 11.
- 493 Zhang, X., Feng, S., Zhang, H., & Yuan, J. (2020). Developing distributed pv in beijing: Deployment potential and economics. *Frontiers in Energy
494 Research*, 7, 155.
- 495 Zhang, Y., Hu, S., Guo, F., Mastrucci, A., Zhang, S., Yang, Z., & Yan, D. (2022). Assessing the potential of decarbonizing china's building
496 construction by 2060 and synergy with industry sector. *Journal of Cleaner Production*, (p. 132086).
- 497 Zomer, C., & Rüther, R. (2017a). Simplified method for shading-loss analysis in bipv systems – part 1: Theoretical study. *Energy and Buildings*,
498 141, 69–82.
- 499 Zomer, C., & Rüther, R. (2017b). Simplified method for shading-loss analysis in bipv systems. part 2: Application in case studies. *Energy and
500 Buildings*, 141, 83–95.